Colloid Polym Sci (2009) 287:231–236
DOI 10.1007/s00396-008-1968-x

SHORT COMMUNICATION

Hierarchies in the structural organization of spider silk—a quantitative model

Periklis Papadopoulos · Jan Sölter · Friedrich Kremer

Received: 8 October 2008 / Revised: 12 November 2008 / Accepted: 13 November 2008 / Published online: 3 December 2008

Abstract The unsurpassed mechanical properties of major ampullate spider silk are *quantitatively* explained by a hierarchical model of its structural organization. Based on combined time-resolved mechanical and Fourier-transform infrared measurements, we show that the core of native silk fibers is strongly prestressed. The prestress is released during wetting, allowing the fibers to shrink, changing permanently the mechanical properties. Prestress is, therefore, the controlling parameter of silk properties.

Keywords FTIR · Major ampullate · Supercontraction

Introduction

The mechanical properties of spider major ampullate (dragline) silk are superior to any other natural and artificial fibers [1]. Numerous experimental techniques have been employed for the study of natural and regenerated spider silk, namely mechanical measurements [2–6], X-ray microscopy [7], X-ray scattering [8–12], nuclear magnetic resonance [13–15], infrared [16, 17], and Raman spectroscopy [18, 19]. Comparison of silkworm and spider silk reveals that both materials have a similar morphology [15, 18–20]. There is consensus that they have hard crystalline β-sheets and soft amorphous segments; however, the structural organization in the amorphous phase is not understood. A recent study on silkworm silk [21] suggests that the crystals are in a serial arrangement with the amorphous phase and are deformed by the application of stress.

Early works usually assumed that stiff crystal regions are connected by coils leading to a material that resembles reinforced rubber [22, 23], but more recent studies prove the existence of oriented and non-oriented regions in the amorphous phase [9, 13, 24, 25] and suggest a three-phase model of spider silk. The amorphous matrix is composed of both extended and helical structures with different numbers of hydrogen bonds per amino acid. A fibrilar structure is also suggested [14, 25]. The high toughness is attributed to hydrogen bond breaking within these regions [5, 26]. Stretching is suggested to convert the glassy amorphous matrix to rubber-like. A skin–core structure of the fiber consisting of fibrils has been also proposed [14]. The interplay of the phases of major ampullate silk and the order of the amorphous parts are correlated to the "supercontraction" on addition of liquid water [27, 28]. Attempts to model other silk types require parameters that cannot be directly related to microscopic quantities [29]. Despite some success of these models, no *quantitative* theory exists which links for both native and supercontracted major ampullate silk the microscopic molecular properties to the well-known macroscopic mechanical findings.

Recently, we carried out combined mechanical and Fourier-transform infrared (FTIR) spectroscopic measurements on major ampullate silk of *Nuctenea sclopetaria* spiders [30]. The observation of a linear *thresholdless* dependence for the frequency of β-sheet-specific vibrations on stress is explained using quantum mechanical perturbation theory by treating the mechanical stress as a weak disturbance of the molecular oscillations. Due to the anharmonicity of the potential describing main-chain oscillations, first-order perturbation terms give rise to a decrease of vibrational energy levels, which is proportional

P. Papadopoulos (✉) · J. Sölter · F. Kremer
Institut für Experimentelle Physik I, Universität Leipzig,
Linnéstraße 5,
04103 Leipzig, Germany
e-mail: papadopoulos@physik.uni-leipzig.de

to the force which is applied to the respective bonds. By that, a microscopic probe of stress *within* the β-sheeted crystals is provided. In case of low-order amorphous structures, the mechanical field is no more parallel to the bonds and causes conformational changes instead of bond stretching. The effect is absent in that case, allowing the technique to differentiate between crystalline and amorphous moieties.

Based on this, in the present study, we investigate the interconnection of crystalline and amorphous phases in quantitative detail by comparing native and supercontracted samples. The analysis shows that native silk fibers are significantly prestressed in contrast to the supercontracted ones. The silk mechanical properties may be described by a structural model which consists of alanine-rich β-sheeted crystals interlinked by prestrained glycine-rich amorphous chains. Assuming that the chains have a Gaussian distribution of prestrain and obey the worm-like chain (WLC) model [31], the complete stress–strain curves can be delivered. The change of the prestrain distribution explains why such differences in the mechanical properties are observed, despite the fact that no fundamental change of the microscopic structure occurs.

Experimental

The samples are major ampullate silk from *Nephila madagascariensis* spiders, obtained by forced milking at a speed of ~1 mm/s, room temperature of 23±1 °C and relative humidity of 50±10%. The silk fiber is double (from the two major ampullate glands) and 200 turns are wound around two metal rods in order to form a 6-mm-long dense double-layer grid. Fiber thickness at zero strain is measured by laser diffraction and atomic force microscopy (AFM) and is found to be 3.3±0.3 μm. Supercontraction is realized by addition of a water droplet to the silk wire grid which is allowed to shrink to the maximum possible extent in a few seconds. Subsequently, it is stored for several days in ambient air in order to reach a content of bound water comparable to that of the native sample as monitored by the amide I, II, and A bands.

The same setup and analysis procedure as in our previous publication are applied [30]. A Bio-Rad FTS 6000 spectrometer with a liquid-nitrogen-cooled MCT-PV detector with excellent linearity working in the range from 800 to 5,000 cm^{-1} at a resolution of 1 cm^{-1} is used for the FTIR measurements. A KRS-5 IR polarizer is inserted in the IR beam in order to study the dichroism of certain absorption bands (Fig. 1a). During the FTIR measurements, the force applied to the sample is measured using a Burster 8411-10 sensor, capable of measuring forces up to 10 N with an error of 0.25%. Temperature and RH throughout the measurements are in the same ranges as in the milking

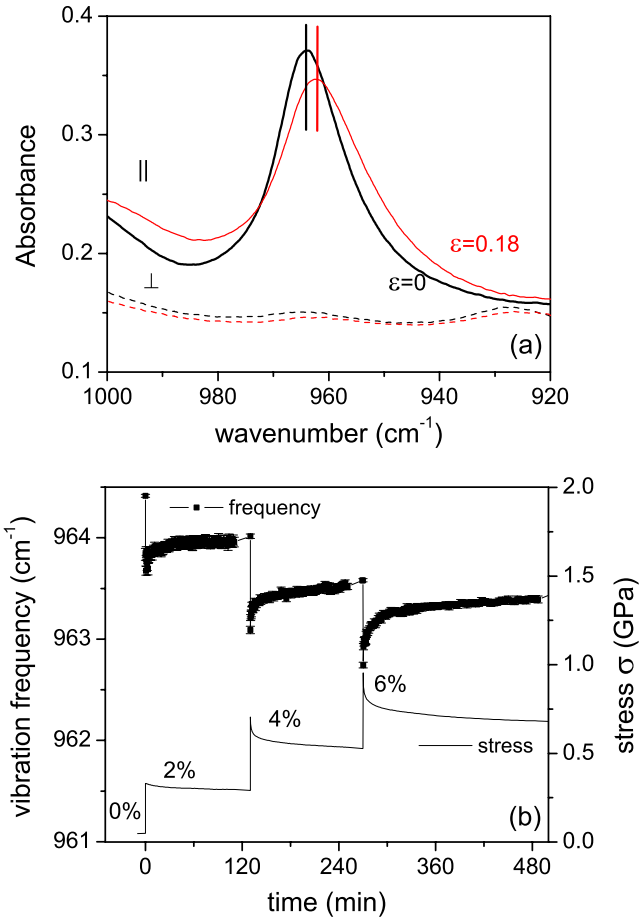

Fig. 1 Frequency shift of a β-sheet polyalanine-specific vibration. **a** The high alignment of the crystals is revealed using light polarized parallel and perpendicular to the fibers. Increasing strain ε shifts the frequency to lower wavenumbers. **b** The shift follows the force relaxation after the stepwise strain increase. *No threshold* is observed. Equilibrium is reached typically after 2–3 h at room temperature

procedure. The spider silk wire grid can be stretched with 2-μm screws with an accuracy of 5 μm. Strain is increased stepwise and kinetic measurements (with light polarized parallel to the fibers) are carried out while the force relaxes (Fig. 1b). Static polarization-dependent measurements are started when equilibrium is reached (typically 2–3 h after the step). The obtained stress–strain curve refers to the equilibrium measurements and shows some differences from measurements carried out with a constant stretching rate. Stress values presented herein refer to the true stress, which is calculated assuming constant silk fiber volume throughout the measurements.

Results

The alanine-rich crystals in native silk are highly oriented along the fiber axis as proven by the dichroism of the

polyalanine-specific vibration at 965 cm^{-1} in native silk (Fig. 1a). The band is shifted continuously to lower wavenumbers by increasing the stress on the fiber. This holds for equilibrated and dynamic experiments. The latter experiment shows "overshoots" after strain increase, typical of viscoelastic materials [21], which are accompanied by "undershoots" of the vibrational frequency (Fig. 1b). As described above, the effect is the consequence of the external perturbation on anharmonic oscillators and is observed for all main-chain crystal vibrations.

The shift of the polyalanine vibration shows a linear *thresholdless* dependence on the applied macroscopic stress, regardless of the strain (for kinetic and equilibrated measurements) (Fig. 2a), proving that the alanine-rich β-sheeted crystals and the amorphous phase are in a serial arrangement. The average microscopic stress is equal to the macroscopic stress under equilibrium conditions, but strong deviations would be observed in dynamic measurements if the force was transferred through the entanglements, bypassing the crystals. Similar findings are observed for the alanine–glycine moieties located at the boundaries of the β-sheeted crystals [32, 33], which give rise to a band around 1,000 cm^{-1}. The molecular-order parameter for both amino acid residues $(Ala)_n$ and $(AlaGly)_n$ is close to 1 (Fig. 1b).

The amorphous regions between the β-sheeted crystals assume the polyglycine I (vibration at ~1,015 cm^{-1}) and polyglycine II (at ~1,026 cm^{-1}) conformations, constituting approximately 25% and 30%, respectively, of silk. Despite the fact that they do not show a stress-dependent shift of their mean spectral position (Fig. 2a), the non-zero and increasing order parameter is an indication that the chains are prestrained.

The linear frequency shift dependence is also observed for the supercontracted sample, showing that the nano-phases are still in serial arrangement, even though the mechanical properties change dramatically. However, during supercontraction, under almost zero macroscopic stress (<0.05 GPa), the alanine moieties show a frequency shift to higher wavenumbers, indicating release of stress (Fig. 2a). In contrast, the molecular-order parameter remains the same for both samples—after a weak orientational effect at low stress (Fig. 2b). This is a proof of the existence of prestress, which does not allow the crystals to decrease their orientational entropy. This prestress is not released completely, even after wetting.

The above experimental findings can be quantitatively described by the following structural model (Fig. 3) for both native and supercontracted major ampullate silk: (1) the alanine-rich β-sheeted crystals are assumed to be interlinked by glycine-rich amorphous chains having (2) a Gaussian distribution of prestrain and obeying (3) the WLC model [31]. Hereby, the internal pressure due to the

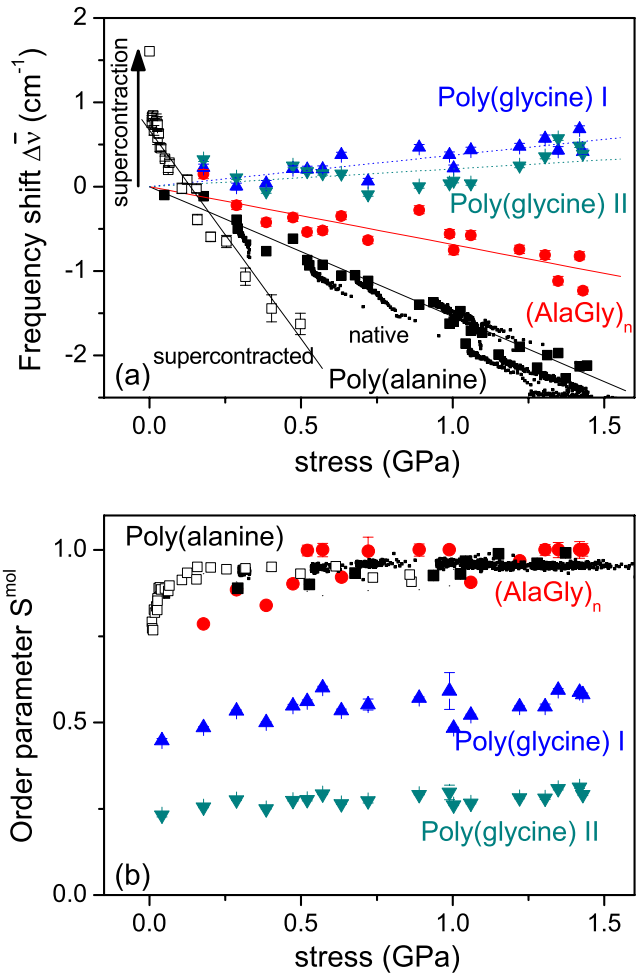

Fig. 2 Microscopic effects of stress. **a** A linear frequency dependence on stress is observed for the alanine-rich crystal vibrations (*black* and *red symbols*), whereas amorphous structures show no trend (*blue* and *green symbols*). In the first case, linearity is obeyed in both kinetic (*small symbols*) and equilibrium conditions (*large symbols*). A shift to higher wavenumbers reveals a release of prestress during supercontraction (*open symbols*). The length of the *error bars* is comparable to the size of the symbols, in most cases. **b** The crystals are highly oriented, whereas the glycine-rich amorphous chains exhibit lower order. Supercontraction allows partial reorientation of the crystals, which is reversed by re-stretching. No difference is observed under non-equilibrium conditions

prestrained chains in the amorphous phase is (4) counterbalanced by the skin in the core periphery [14, 34]. The effect of supercontraction is unambiguously explained by this model due to a dramatic decrease of the elastic modulus of the skin and the core periphery upon wetting with water. This leads to a decrease of the internal pressure and a negative shift of the frequency position of the alanine band as observed experimentally. We should mention here that the serial arrangement of phases exists only in the core. The skin is in "parallel" connection and explains the difference between microscopic (core) and macroscopic stress the first time it is wetted. Its contribution is minimal thereafter.

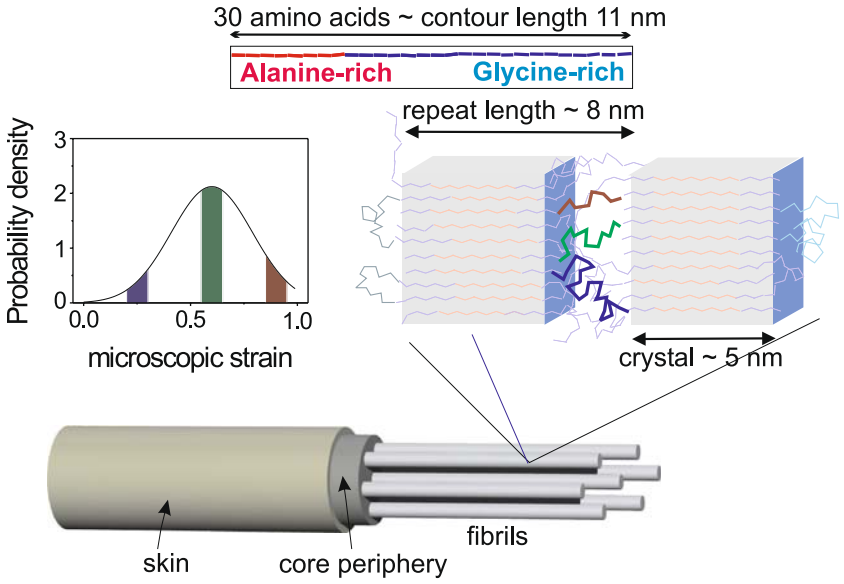

Fig. 3 Model of aligned crystals connected by pre-stressed chains having a broad gaussian distribution of pre-stress. In addition to the FTIR measurements, the model is based on X-ray results [9, 12] giving the crystal dimensions and spacing. This nanostructure composes the nanofibrils which are wrapped in the skin [14] which counterbalances the core prestress. The model has only two adjustable parameters

The proposed model has besides some known geometrical features [9, 12] only *two* adjustable parameters, the mean value and the width of the Gaussian distribution of prestrain λ_m:

$$p(\lambda_m) = \frac{1}{w\sqrt{2\pi}} e^{-\frac{(\lambda_m-\mu)^2}{w^2}} \quad (1)$$

where μ is the average prestrain and w the distribution width. The amorphous chains can be modeled as worm-like ones

$$f_{wlc}(\lambda_m) = \frac{k_B T}{l_p}\left(\frac{1}{4(1-\lambda_m)^2} - \frac{1}{4} + \lambda_m\right) \quad (2)$$

where f_{wlc} is the force on a single chain. The persistence length l_p is estimated by AFM measurements to ≈0.4 nm [35]. During stretching under quasi-static conditions, all chains are stretched uniformly and the prestrain distribution changes following the relation

$$\lambda'_m(\varepsilon) = \lambda_m(1+\varepsilon)\left(\frac{1}{f_{amorphous}} - 1\right) \quad (3)$$

where ε is the macroscopic strain and $f_{amorphous}$ is the length fraction of amorphous chains. The elastic modulus of the crystals is currently not known, but there are strong indications that it is much higher than that of the amorphous phase [21, 23]; so their elasticity is neglected here. The value of $f_{amorphous}$ is determined from X-ray measurements and is found close to 0.38 [9, 12, 14, 36]. The total stress is calculated by integration from zero to the maximum limit $\lambda_r \approx 0.99$ of prestrain. The physical meaning of this limit is that chains exceeding this strain are peeled off the crystals [35] and have a negligible prestrain thereafter. Splitting of crystals in silk has been recently suggested as a possible way of energy dissipation [8].

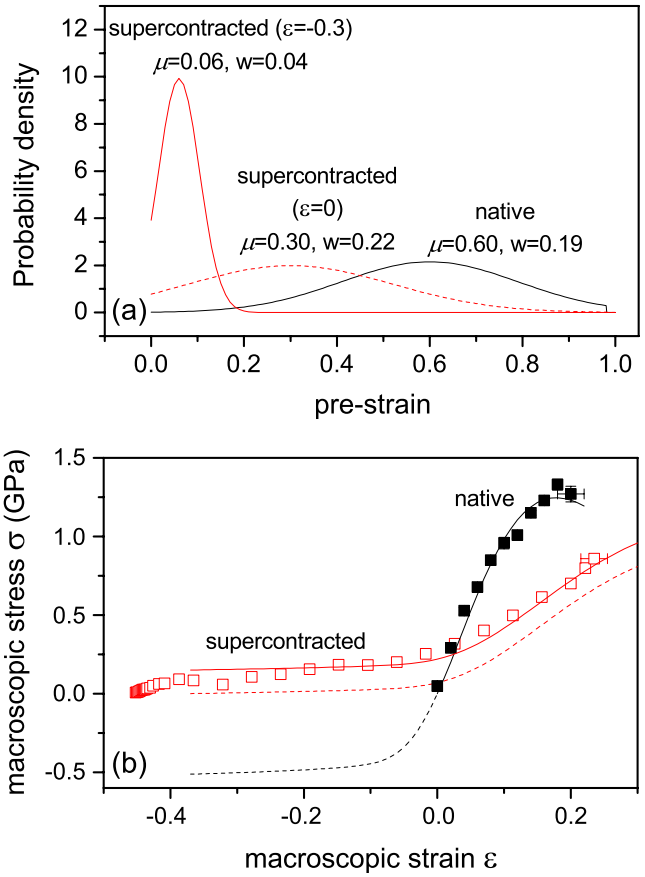

Fig. 4 Dependence of the mechanical properties of silk on the prestress. **a** The model can describe both native and supercontracted states assuming different prestrain distributions ($\mu = 0.60, w = 0.19$ and $\mu = 0.30, w = 0.22$, respectively, at ε=0). **b** Fit of experimental data at equilibrium conditions with the model. A constant vertical offset σ_0 has been added to the stress curves, showing the contribution of the fiber skin. Notice the prediction of a prestress of 0.5 GPa in native silk. The model is not valid at low strain, where the crystals are not perfectly oriented (see Fig. 2b)

The final term that needs to be included in the stress–strain equation is the contribution of the fiber skin. The internal prestress at zero strain in native silk, σ_0, must be counterbalanced there; otherwise, the fiber would collapse. Wetting of silk softens the skin and allows the fiber to shrink. We assume that this contribution is constant because no deviations from linearity in Fig. 2 are observed, except during supercontraction. The final equation giving the fiber stress is

$$\sigma(\varepsilon) = \frac{1}{A_{\text{chain}}} \int_0^{\lambda_r} p\left(\lambda'_{\text{m}}(\varepsilon)\right) f_{wlc}\left(\lambda'_{\text{m}}(\varepsilon)\right) d\lambda_{\text{m}} - \sigma_0 \qquad (4)$$

where A_{chain} is the cross section of a single chain in β-sheets (0.20 nm^2) [10].

The model can describe both states assuming different initial distributions of prestress (Fig. 4). The distribution collapses to zero during supercontraction and, even after stretching to the original length, the average prestress is lower than the native sample. The decreased prestress is responsible for the lower elastic modulus and greater extensibility of supercontracted silk. This result explains why humidity may affect significantly the mechanical properties [37, 38].

We mention here that the model can describe the equilibrated state of silk; therefore, the experimental stress–strain curves in Fig. 4b are obtained from measurements after the slow force relaxation is complete (average strain rate $<10^{-3}$ s^{-1}). Relaxation becomes more significant at high strain values (Fig. 1b), causing deviations at higher strain rates.

The high toughness, that is the energy absorbed until rupturing $\left(\approx 200\text{MJ}/\text{m}^3\right)$, is comparable to the total energy of hydrogen bonds in the crystals. Using parameters similar to a mean field silk model [5] (one hydrogen bond per amino acid with energy of 10 kJ mol^{-1}, density of 1.3 g cm^{-3}, and average molecular weight of 70 g mol^{-1}), the energy of the crystals (f=0.45) is ≈85 MJ m^{-3}, whereas the ordered amorphous regions (f=0.25) have only ≈45 MJ m^{-3}. Therefore, the toughness is attributed primarily to the breaking of hydrogen bonding in the crystals [8]. When the microscopic strain of an amorphous chain exceeds a certain limit, it is peeled off the crystal and the polyalanine block may be connected to another one in a more relaxed conformation.

Conclusions

In conclusion, combined time-resolved mechanical and polarized Fourier-transform infrared measurements allow us to unravel the different levels of structural organization in major ampullate spider silk in the native and supercontracted state. The most important finding is that the measurable prestress is the controlling quantity of the mechanical properties. The internal prestress is counterbalanced by the fiber skin and the core periphery and is released during supercontraction. The high prestress in native silk leads to a material with high elastic modulus. On the other hand, the much lower prestress in supercontracted silk decreases the modulus and allows for greater extensibility. Assuming highly aligned alanine-rich β-sheeted crystals which are interconnected by glycine-rich worm-like chains having a Gaussian distribution of prestrain, the macroscopic stress–strain dependence can be described. The extraordinary toughness of spider silk can be explained by the breaking of hydrogen bonds within the crystalline regions.

Miscellaneous We would like to thank Prof. Fritz Vollrath (Oxford University) and Dr. Alex Sponner (Institute of Entomology, Češke Budejovice) for fruitful discussions and helpful comments on this work.

References

1. Kubik S (2002) High-performance fibers from spider silk. Angew Chem Int Ed 41:2721–2723
2. Holland C, Terry AE, Porter D et al (2007) Natural and unnatural silks. Polymer 48:3388–3392
3. Seidel A, Liivak O, Calve S et al (2000) Regenerated spider silk: processing, properties, and structure. Macromolecules 33:775–780
4. Swanson BO, Blackledge AA, Beltran J et al (2006) Variation in the material properties of spider dragline silk across species. Appl Phys A 82:213–218
5. Porter D, Vollrath F, Shao Z (2005) Predicting the mechanical properties of spider silk as a model nanostructured polymer. Eur Phys J E 16:199–206
6. Thiel BL, Guess KB, Viney C (1997) Non-periodic lattice crystals in the hierarchical microstructure of spider (major ampullate) silk. Biopolymers 41:703–719
7. Glišović A, Thieme J, Guttmann P et al (2007) Transmission X-ray microscopy of spider dragline silk. Int J Biol Macromol 40:87–95
8. Glišović A, Vehoff T, Davies RJ et al (2008) Strain dependent structural changes of spider dragline silk. Macromolecules 41:390–398
9. Grubb DT, Jelinski LW (1997) Fiber morphology of spider silk: the effects of tensile deformation. Macromolecules 30:2860–2867
10. Riekel C, Vollrath F (2001) Spider silk fibre extrusion: combined wide- and small-angle X-ray microdiffraction experiments. Int J Biol Macromol 29:203–210
11. Parkhe AD, Seeley SK, Gardner K et al (1997) Structural studies of spider silk proteins in the fiber. J Mol Recognit 10:1–6
12. Yang Z, Grubb DT, Jelinski LW (1997) Small-angle X-ray scattering of spider dragline silk. Macromolecules 30:8524–8261
13. Simmons A, Ray E, Jelinski LW (1994) Solid-state ^{13}C NMR of *Nephila clavipes* dragline silk establishes structure and identity of crystalline regions. Macromolecules 27:5235–5237
14. van Beek JD, Hess S, Vollrath F et al (2002) The molecular structure of spider dragline silk: folding and orientation of the protein backbone. Proc Natl Acad Sci USA 99:10266–10271
15. Yang M, Asakura T (2005) Design, expression and solid-state NMR characterization of silk-like materials constructed from sequences of spider silk, *Samia cynthia ricini* and *Bombyx mori* silk fibroins. J Biochem 137:721–729

16. Bramanti E, Catalano D, Forte C et al (2005) Solid state ^{13}C NMR and FT-IR spectroscopy of the cocoon silk of two common spiders. Spectrochim Acta A 62:105–111
17. Dong Z, Lewis RV, Middaugh CR (1991) Molecular mechanism of spider silk elasticity. Arch Biochem Biophys 284:53–57
18. Rousseau ME, Lefèvre T, Beaulieu L et al (2004) Study of protein conformation and orientation in silkworm and spider silk fibers using Raman microspectroscopy. Biomacromolecules 5:2247–2257
19. Sirichaisit J, Brookes VL, Young RJ et al (2003) Analysis of structure/property relationships in silkworm (*Bombyx mori*) and spider dragline (*Nephila edulis*) silks using Raman spectroscopy. Biomacromolecules 4:387–394
20. Shao J, Zheng J, Liu J et al (2005) Fourier transform Raman and Fourier transform infrared spectroscopy studies of silk fibroin. J Appl Polym Sci 96:1999–2004
21. Krasnov I, Diddens I, Hauptmann N et al (2008) Mechanical properties of silk: interplay of deformation on macroscopic and molecular length scales. Phys Rev Lett 100:048104
22. Gosline JM, Denny MW, Demont ME (1984) Spider silk as rubber. Nature 309:551–552
23. O'Brien JP, Fahnestock SR, Yves T et al (1998) Nylons from nature: synthetic analogs to spider silk. Adv Mater 10:1185–1195
24. Rousseau M-E, Cruz DH, West MM et al (2007) *Nephila clavipes* spider dragline silk microstructure studied by scanning transmission X-ray microscopy. J Am Chem Soc 129:3897–3905
25. Sapede D, Seydel T, Forsyth VT et al (2005) Nanofibrillar structure and molecular mobility in spider dragline silk. Macromolecules 38:8447–8453
26. Vollrath F, Porter D (2006) Spider silk as a model biomaterial. Appl Phys A 82:205–212
27. Liu Y, Shao Z, Vollrath F (2005) Relationships between supercontraction and mechanical properties of spider silk. Nature Mater 4:901–906
28. Guinea GV, Elices M, Pérez-Rigueiro J et al (2004) Stretching of supercontracted fibers: a link between spinning and the variability of spider silk. J Exp Biol 208:25–30
29. Zhou H, Zhang Y (2005) Hierarchical chain model of spider capture silk elasticity. Phys Rev Lett 94:028104
30. Papadopoulos P, Sölter J, Kremer F (2007) Structure–property relationships in major ampullate spider silk as deduced from polarized FTIR spectroscopy. Eur Phys J E 24:193–199
31. Kratky O, Porod G (1949) Röntgenuntersuchung gelöster fadenmoleküle. Recl Trav Chim Pays Bas 68:1106–1123
32. Eles PT, Michal CA (2004) A decoder NMR study of backbone orientation in *Nephila clavipes* dragline silk under varying strain and draw rate. Biomacromolecules 5:661–665
33. Lefèvre T, Rousseau M-E, Pézolet M (2007) Protein secondary structure and orientation in silk as revealed by Raman spectromicroscopy. Biophys J 92:2885–2895
34. Sponner A, Vater W, Monajembashi S et al (2007) Composition and hierarchical organisation of a spider silk. PLoS ONE 2:e998
35. Oroudjev E, Soares J, Arcidiacono S et al (2002) Segmented nanofibers of spider dragline silk: atomic force microscopy and single-molecule force spectroscopy. Proc Natl Acad Sci USA 99:6460–6465
36. Gosline JM, Guerette PA, Ortlepp CS et al (1999) The mechanical design of spider silks: from fibroin sequence to mechanical function. J Exp Biol 202:3295–3303
37. Plaza GR, Guinea GV, Pérez-Rigueiro J et al (2006) Thermo-hygro-mechanical behavior of spider dragline silk: glassy and rubbery states. J Polym Sci B Polym Phys 44:994–999
38. Vehoff T, Glišović A, Schollmeyer H et al (2007) Mechanical properties of spider dragline silk: humidity, hysteresis, and relaxation. Biophys J 93:4425–4432